JJEE
Volume 5, Number 3, 2019
Pages 149-160
Jordan Journal of Electrical Engineering
ISSN (Print): 2409-9600, ISSN (Online): 2409-9619

Effective Parameters of Split Rings with Loop Antennas in Homogeneous Lossy Media

Rula S. Alrawashdeh*

Department of Electrical Engineering, Mutah University, Alkarak, Jordan
E-mail: rularsr18@gmail.com

Received: March 31, 2019 *Accepted: May 30, 2019*

***Abstract*—** In this paper, the effective parameters of a metallic layer of rectangular split rings placed on the top of a rectangular loop antenna in a lossy medium are investigated. The equivalent circuit parameters are analyzed; and their effect on the antenna radiation efficiency and gain is discussed. Investigations are conducted in a homogeneous lossy medium. It is found that decreasing each of the length and height of the inner split ring investigated in this paper by 2 mm decreases the transmission coefficient of the loop antenna by 23%. Also, it is found that increasing the strip width of the inner ring by 2 mm decreases the transmission coefficient by 38%. The effect of the equivalent circuit parameters of the split rings on the performance of a loop antenna in a lossy medium is linked to the antenna radiation efficiency and gain for the first time in literature. The results in this paper are very helpful to control the parameters of split rings to increase the power radiated from loop antennas in lossy media.

***Keywords*—** Lossy media; Near electromagnetic fields; Split rings; Transmission coefficient.

1. INTRODUCTION

There are several beneficial applications for antennas in lossy media such as implantable and under-sea applications [1, 2]. The lossy medium absorbs most of the antenna radiation. Therefore, the antenna in the lossy medium has usually small radiation efficiency and gain [3, 4]. Magnetic type antennas are found to outperform electrical type antennas in the nonmagnetic lossy medium which does not present magnetic losses [4]. Hence, loop antennas which are magnetic in type are very popular for applications in lossy media [5, 6]. However, a small ratio of power is usually radiated outside the lossy medium even if loop antennas are used. The radiated power can be increased if an insulation layer is placed between the antenna and lossy medium [4]. However, the insulation layer is usually thin; and its effect on increasing the radiated power is thus limited. The increase in the radiated power is larger for layers based on the split rings than that for typical insulation layers. These layers tend to increase the near magnetic field and antenna gain accordingly [7]. Although using such layers was shown to be promising, it was rarely investigated in literature; and the effect of its split ring parameters has not been investigated in depth. Such investigations are important to exploit the split rings structure effectively to maximize the increase in the radiated power. Hence, such investigations are still needed. Therefore, this paper aims at investigating the effective parameters of the split rings layer and studying how they work to increase the power radiated from the antenna in the lossy medium. This paper is organized as follows: First, the antenna and layer layout structure is presented. Then, effective design parameters of the rings are discussed, via simulations, and linked to equivalent circuit parameters. The

* Corresponding author

measurement results of the optimized structure are also presented. Finally, the paper is concluded.

2. ANTENNA AND LAYER STRUCTURES

A typical rectangular loop antenna has been selected for investigation in this paper. A layer of rectangular split rings has been also selected. The antenna and layer are shown in Fig. 1. The layer has a small thickness of 0.1 mm; and is placed on the top of the antenna. The structure of the antenna and layer is similar to that in [6]. However, the dimensions are increased to obtain resonance at 403 MHz instead of 2.45 GHz. 403 MHz is the center frequency of the 401 – 406 MHz Medical Device Radio communications Service (MedRadio) band which is mainly allocated for implantable applications in the lossy human body [8, 9].

The antenna and layer are flexible. They are bent around a cylindrical implant of 5 mm in radius and 15 mm in length as shown in Fig. 2. The antenna and layer bent around the implant are placed inside a homogenous lossy medium of a relative permittivity (ε_r) of 57, conductivity (σ) of 0.79 S/m and loss tangent ($\tan\delta$) of 0.6226 which resemble the dielectric properties of a human muscle at 403 MHz [10]. The antenna with a layer around the implant is placed at the center of a human body model of an elliptic cylindrical shape which is (180×100×50) mm^3 in size. This model has been particularly selected because it has provided an accurate evaluation of antennas in the lossy human body despite its simplicity [7]. This model is shown in Fig. 3.

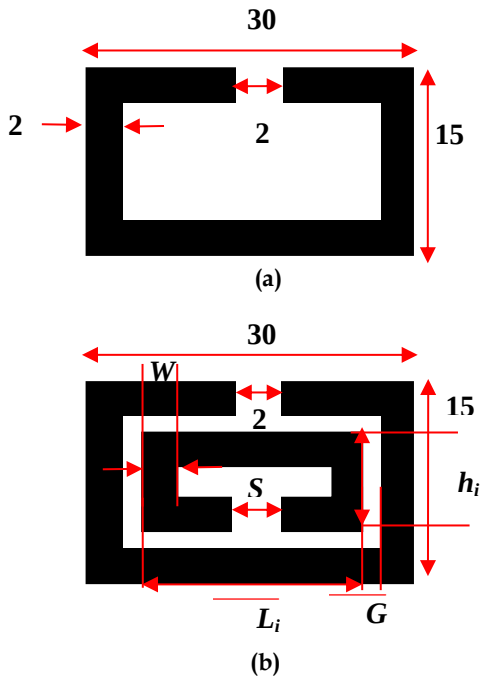

Fig. 1. Layout structures of the: a) antenna; b) layer based on split rings (dimensions: mm).

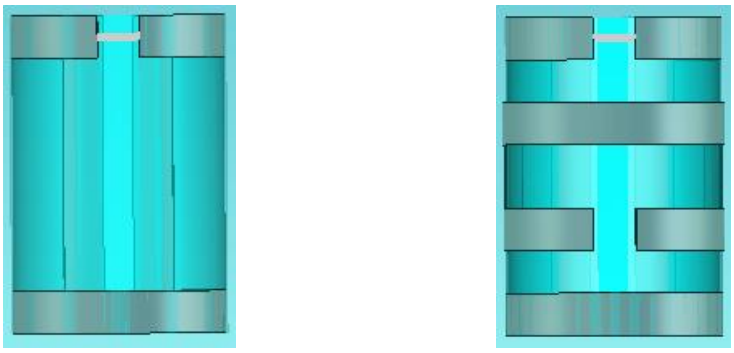

(a) (b)

Fig. 2. Layout structures of the: a) antenna; b) layer based on split rings bent around the cylindrical implant.

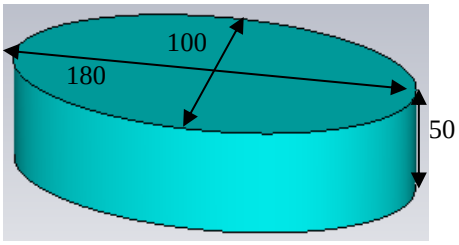

Fig. 3. The investigated lossy model (dimensions: mm).

3. ANALYSIS

The main parameters of investigation in this paper are shown in Fig. 1. These parameters are the: split width (*S*), strip width (*W*), spacing between the rings (*G*), length of the inner split ring (L_i) and height of the inner split ring (h_i). The parameters of the antenna and outer ring have the same dimensions. Only one parameter is varied each time.

The split rings can be modeled as a LC tank circuit [11]. Some of its parameters contribute to the capacitance while others to the inductance. This will be discussed in the following subsections.

3.1. Effect of the Split Width and Spacing between the Rings

Both split width (*S*) and spacing between rings (*G*) are compared to spacing (*d*) between the plates of a parallel plate capacitor. The capacitance C_{pp} [F] of a parallel plate capacitor decreases as this distance increases as shown in Eq. (1) [12]:

$$C_{pp} = \frac{\varepsilon A_{plate}}{d} \quad (1)$$

where ε [F/m] is the permittivity of the dielectric material between the plates; and A_{plate} [m²] is the plate area.

When the split width and spacing between the rings increase, the antenna radiation efficiency increases. This is because the near electric field decreases. When the near electric field $|E|$ [V/m] decreases, the power absorbed P_{abs} [W] by the surrounding lossy media is decreased. Consequently, the total radiated power P_{rad} [W] and radiation efficiency (η_e) increase as shown in Eqs. (2-4) [4].

$$P_{in} = P_{abs} + P_{ref} + P_{rad} \quad (2)$$

where P_{in} [W] is the total input power; and P_{ref} [W] is the reflected power.

$$P_{abs} = \frac{\omega}{2} \iiint \varepsilon_0 \varepsilon_e{}'' |E|^2 dv \quad (3)$$

where ω [rad/sec] is the radian frequency; ε_0 [F/m] is the free space permittivity; $\varepsilon_e{}''$ is the imaginary part of the complex effective permittivity of the lossy medium.

$$\eta_e = \frac{P_{rad}}{P_{in}} \quad (4)$$

The decrease of the near electric field resembles the decrease of the total capacitance of the rings which is obtained when the split width and spacing between the rings increase.

The resonant frequency f_r [Hz] is shifted down when either *S* or *G* decreases. The effective capacitance C_{eff} [F] increases for this case. When it increases, the resonant frequency is shifted down as in Eq. (5) [11]:

$$f_r = \frac{1}{2\pi\sqrt{L_{eff}C_{eff}}} \quad (5)$$

where L_{eff} [H] is the total effective inductance.

3.2. Effect of Length and Height of the Inner Loop

When the length and height of the inner ring increase, the antenna gain (G_{con}) is increased. The near magnetic field $|H|$ [A/m] accordingly increases as shown in Eq. (6) [3]. In like manner, the effective inductance of the circuit increases as shown in Eq. (7) [13, 14].

$$G_{con} = \frac{4\pi\sqrt{\left(\frac{\omega\mu}{2\sigma}\right)}\left(|H|d'e^{\left(\frac{d}{\delta}\right)}\right)^2}{R_r(i_i)^2} \quad (6)$$

where d' [m] is the distance at which $|H|$ is taken or measured; μ [H/m] is the permeability; σ [S/m] is the conductivity; δ [m] is the skin depth; R_r [Ω] is the radiation resistance; and i_i [A] is the input current.

$$L_{eff} = \frac{\mu_0\mu_r}{\pi}\left[-2(L_i + h_i) + 2\sqrt{\left({h_i}^2 + {L_i}^2\right)} - h_i ln\left(\frac{h_i + \sqrt{\left({h_i}^2 + {L_i}^2\right)}}{L_i}\right)\right.$$
$$\left. - L_i ln\left(\frac{L_i + \sqrt{\left({h_i}^2 + {L_i}^2\right)}}{h_i}\right) + h_i ln\left(\frac{2h_i}{\frac{W}{2}}\right) + L_i ln\left(\frac{2L_i}{\frac{W}{2}}\right)\right] \quad (7)$$

where μ_r is the relative permeability; and μ_0 [H/m] is the free space permeability.

When the length and height of the inner ring increase, the total effective inductance increases. As the total effective inductance increases, the resonant frequency is shifted down.

3.3. Effect of the Strip Width

Referring to Eq. (7), the effective inductance decreases when the strip width (*W*) increases. This is reflected on decreasing the near magnetic field and gain with reference to Eq. (6) [3].

The effect of the split rings parameters can be summarized as follows:

- The antenna radiation efficiency increases when the effective capacitance of the rings decreases. This is obtained when the split width (S) and spacing between the rings (G) increase. The decrease in the effective capacitance is linked to the decrease in the near electric field which reduces the power loss due to absorption. When the absorbed power is reduced, the power radiated out from the human body and radiation efficiency increases.
- The antenna gain is increased when the effective inductance of the rings increases. This is obtained when the Length (L_i) and height (h_i) of the inner ring increase and when the width of the strip (W) decreases. The increase in the effective inductance is linked to the increase of the near magnetic field. When the near magnetic field is increased, the antenna gain increases.
- The resonant frequency is shifted down when the equivalent inductance or/and capacitance increase. This is obtained when the split width (S) or/and spacing between the rings (G) decrease and when the length (L_i) and height (h_i) of the inner ring increase. The resonant frequency is shifted up when the strip width (W) increases.

4. VALIDATION

In this section, the effect of the split rings parameters discussed in the previous section is validated via simulation and measurements. The reflection coefficient, near electromagnetic fields and transmission coefficient are simulated. The simulation results are evaluated in correspondence to the analysis in the previous section. Simulations are conducted via the simulation package CST Microwave Studio [15]. Hexahedral meshes are employed; and a minimum distance of $\lambda/4$ is kept between the structure and the edge of the simulation space. The antennas are fed by discrete ports of 50 Ω with an input power of 1 W. The reflection and transmission coefficients are also measured; and the results are compared with the simulation results.

4.1. Effect of the Split Rings Parameters on the Resonant Frequency

The effect of the split ring parameters on the resonant frequency is evaluated by simulating the reflection coefficient. The following parameters are investigated: spacing between the rings (G), strip width (W) and split width (S). When the length (L_i) and height (h_i) of the inner ring are increased or decreased while maintaining the dimensions of the outer ring, spacing between rings (G) is decreased or increased, respectively. Hence, the effect of the length and height of the inner ring on the resonant frequency is the same as that for the spacing between rings.

The simulated reflection coefficient for three values of the spacing between the rings (G = 0.5 mm, 1 mm and 1.5 mm) is shown in Fig. 4. It can be seen from the figure that the smallest resonant frequency (f_r = 313 MHz) is obtained for G = 0.5 mm because the largest equivalent capacitance is obtained for this value of G. The resonant frequency is shifted up by 11 MHz when G is increased from 0.5 to 1.5 mm.

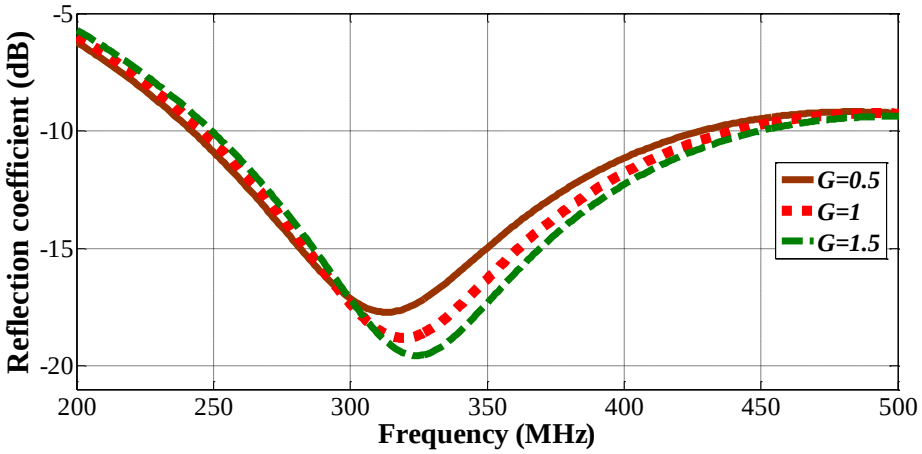

Fig. 4. The reflection coefficient S_{11} for different values of spacing between the rings.

The simulated reflection coefficient for three values of the strip width (W = 1 mm, 2 mm and 3 mm) is shown in Fig. 5. It can be seen from the figure that the resonant frequency is shifted up by 33 MHz (from 302 to 335 MHz) when the strip width is increased by 2 mm (from 1 to 3 mm). This is because the effective inductance is decreased when the strip width is increased.

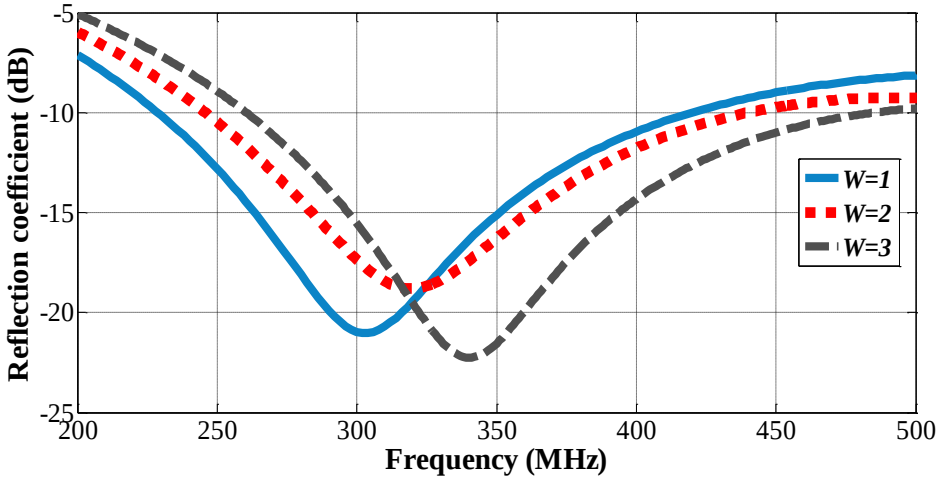

Fig. 5. The reflection coefficient S_{11} for different values of the strip width.

The reflection coefficient for three values of the split width (S = 2 mm, 4 mm and 6 mm) is shown in Fig. 6. It can be seen from the figure that the resonant frequency is shifted up by 10 MHz (from 321 to 331 MHz) when the split width is increased by 4 mm (from 2 to 6 mm). This is because the effective capacitance is decreased when the split width is increased.

The results in this section match very well with the analysis in the previous section. While deep matching (S_{11}<-10dB) is obtained for all the parameters investigated in this subsection, other characteristics such as the radiated power which is evaluated via the transmission coefficient are mainly considered for selecting the optimum parameters. For example, the strip width is optimized at W = 2 mm although deeper matching is obtained at 403 MHz for W = 3 mm. The transmission coefficient for W = 3 mm is smaller than that for W = 2 mm as shown in the following subsection.

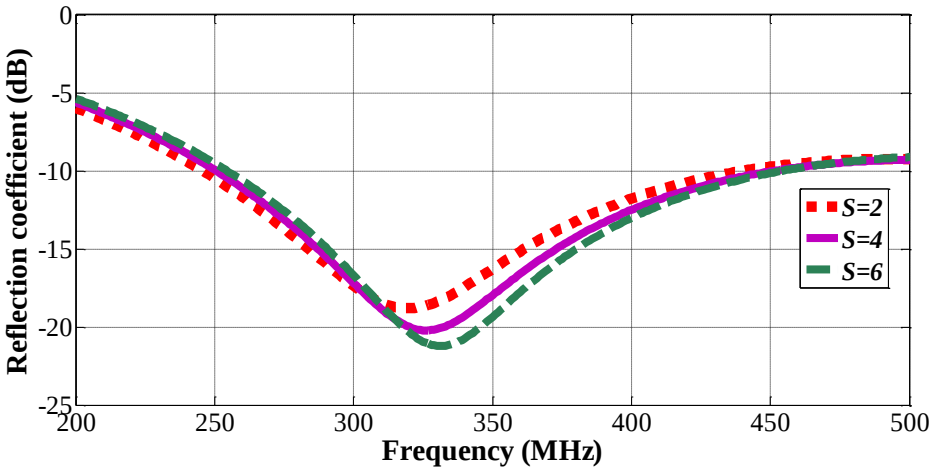

Fig. 6. The reflection coefficient S_{11} for different values of the split width.

4.2. Effect of the Split Rings Parameters on the Transmission Coefficient and Near Electromagnetic Fields

The parameters in the above subsection have been controlled carefully to obtain the maximum possible radiation efficiency and gain and to obtain deep matching (S_{11}< -10 dB) at 403 MHz. The final parameters are summarized in Table 1.

Table 1: Dimensions of the optimized split ring layer parameters.

Parameter	Symbol	Dimension [mm]
Split width	S	2
Strip width	W	2
Spacing between the rings	G	1
Length of the inner ring	L_i	24
Height of the inner ring	h_i	9

The fabricated antenna and layer are shown in Fig. 7. The antenna is made of a copper tape. It is measured in a liquid phantom which is prepared from water, salt and sugar. The ingredients are controlled to obtain $\varepsilon_r = 57$ and $\sigma = 0.79$ S/m which are measured using Agilent 85070E Dielectric Probe [16]. The antenna is wrapped around a cylindrical object of 5 mm in radius and 15 mm in length. An insulation layer is wrapped around the split rings layer during measurements to mitigate the cable effect and provide accurate measurement results. This liquid phantom is shown in Fig. 7. The antenna obtains deep matching (S_{11}< -10 dB) at 403 MHz. The simulated and measured reflection coefficients are shown in Fig. 8. The measured results are in good agreement with the simulated results. Deeper matching is obtained for measurements at around 403 MHz. However, deep matching (S_{11}< -10 dB) is always obtained for both cases at around this frequency.

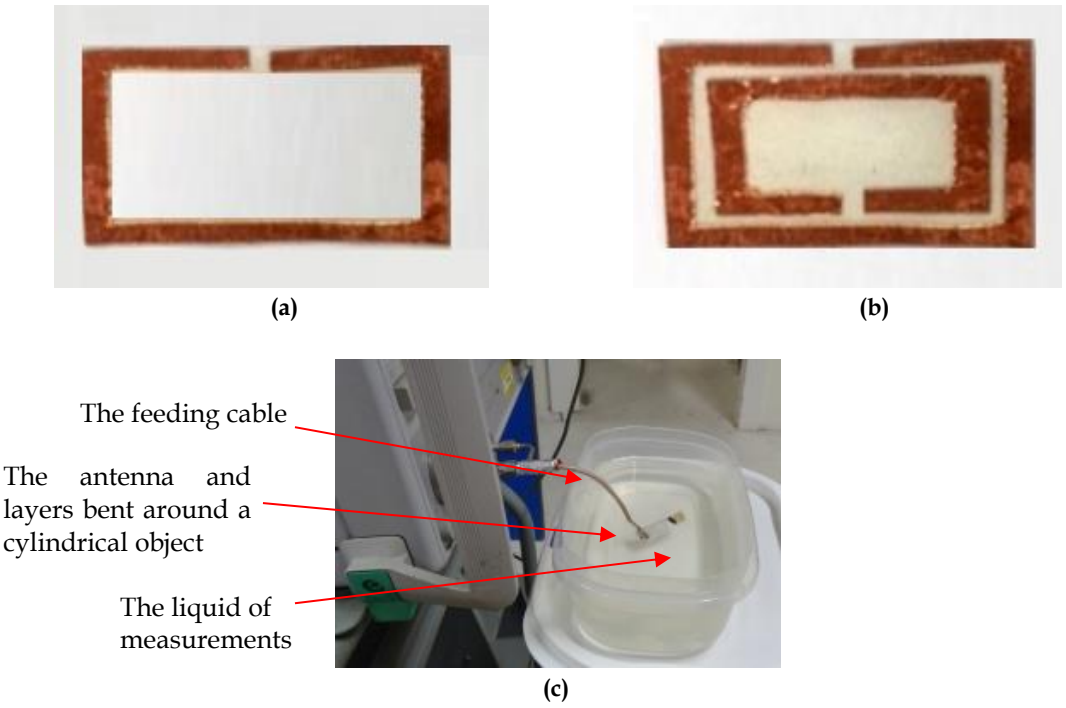

Fig. 7. Measurement setup: a) fabricated antenna; b) fabricated split rings layer; c) liquid phantom, mimicking the lossy model.

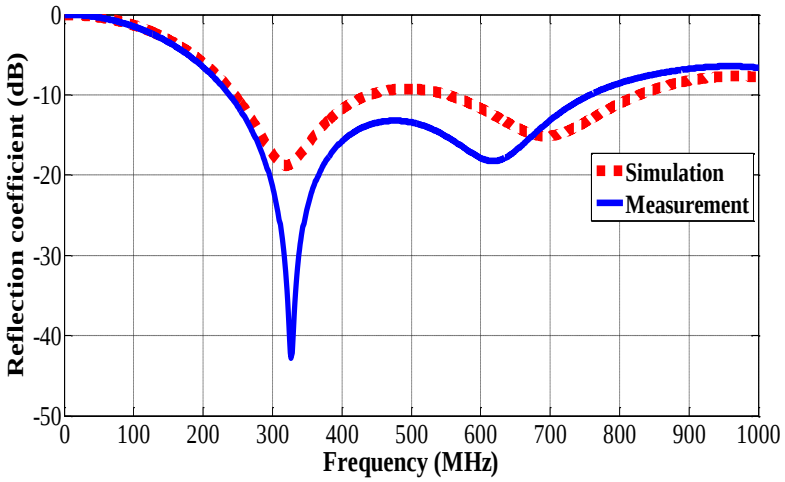

Fig. 8. The simulated and measured reflection coefficient S_{11} for the antenna with the split ring layer investigated in this paper.

The near electric and magnetic fields are computed inside the lossy medium for different combinations of the split ring parameters. These combinations are summarized in Table 2. Please, note that the combination number 0 stands for the optimized parameters in Table 1. The transmission coefficient is computed at 403 MHz at a distance of 2.5 m between the proposed antenna and the meandered loop antenna proposed in [7] in a free space for different combinations of the split ring parameters. The reduction in the transmission coefficient for these combinations in comparison with that for the optimum parameters is summarized in Table 2. The change in the near electromagnetic fields is also indicated. The results in the table show that the transmission coefficient decreases when the length (L_i) and height (h_i) of the inner ring decrease. It also decreases when the strip width of the inner ring increases because the

total inductance decreases. When spacing between the rings (G) increases, the reduction in the transmission coefficient becomes smaller (compare the results in the third row with those in the second row of the table); and capacitance between the rings decreases. This agrees very well with the analysis provided in this paper. As stated above, the variations in the inductance and capacitance are reflected on the near electric and magnetic field variations. The variations in these fields are indicated in Table 2. These variations are corresponding to the variations in the inductance and capacitance claimed in this paper.

Table 2: A comparison between the transmission coefficient and near electromagnetic fields for the optimum and other split rings parameters.

Parameters' combinations		Indication of change of the near electromagnetic fields		Percentage reduction in the transmission coefficient [%]
No of Combination	(S, W, G, L_i, h_i) [mm]	Electric field	Magnetic field	
1	(2, 2, 1, 23, 8)	No change	Decrease	12
2	(2, 2, 1, 22, 7)	No change	Decrease	23
3	(2, 2, 2, 22, 7)	Decrease	Decrease	18
4	(2, 3, 2, 22, 7)	Decrease	Decrease	37
5	(2, 4, 2, 22, 7)	Decrease	Decrease	50
6	(2, 3, 1, 24, 9)	No change	Decrease	23
7	(2, 4, 1, 24, 9)	No change	Decrease	38
8	(1, 4, 1, 24, 9)	Increase	Decrease	41
9	(3, 4, 1, 24, 9)	Decrease	Decrease	35

The normalized transmission coefficient and near electromagnetic fields for these combinations are shown in Figs. 9 and 10, respectively.

The transmission coefficient and near magnetic field are normalized to the maximum value that is obtained for the optimum parameters summarized in Table 1. The near electric field is normalized to its maximum value obtained for combination number 8.

The transmission coefficient (S_{21}) is used to quantify power transmission as in Eqs. (8, 9) [17].

$$|S_{21}|^2 = \frac{P_r}{P_t} \tag{8}$$

where P_t [W] and P_r [W] are the transmitted and received power, respectively.

$$|S_{21}|^2 = \frac{G_t G_r {\lambda_0}^2}{(4\pi R)^2}(1 - |S_{11}|^2)(1 - |S_{22}|^2)e_p \tag{9}$$

where G_t and G_r are the gain of the transmitting (the loop with the split rings layer) and receiving (meandered loop) antennas, respectively. G_t varies for different combinations; G_r is 2.15 dB at 403 MHz for the receiving meandered loop antenna [7]; λ_0 [m] is the free space wavelength which is calculated at 403 MHz; S_{11} and S_{22} are the reflection coefficients of the transmitting and receiving antennas which are smaller than -10 dB for the well-matched transmitting and receiving antennas in this paper; R [m] is the spacing between the transmitting and receiving antennas which is 2.5 m

for this case; and e_p is the polarization mismatch factor which is considered to be unity. The transmission coefficient is only affected by the variation of G_t for this case as all other parameters are kept fixed.

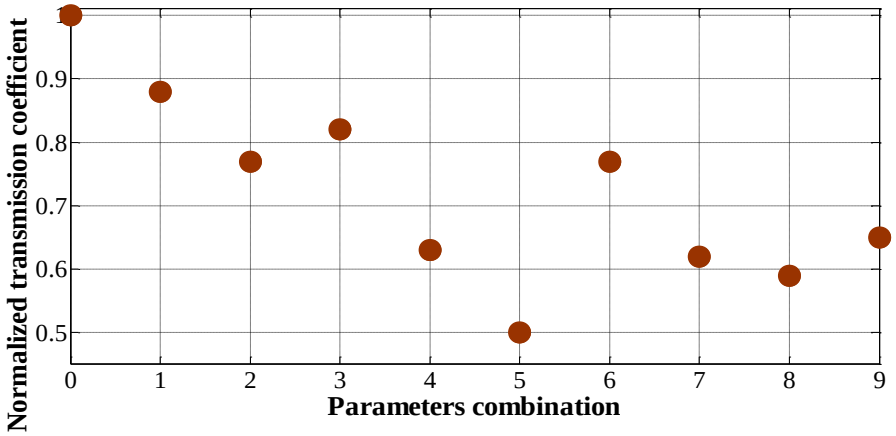

Fig. 9. The normalized transmission coefficient for the parameter combinations summarized in Table 2.

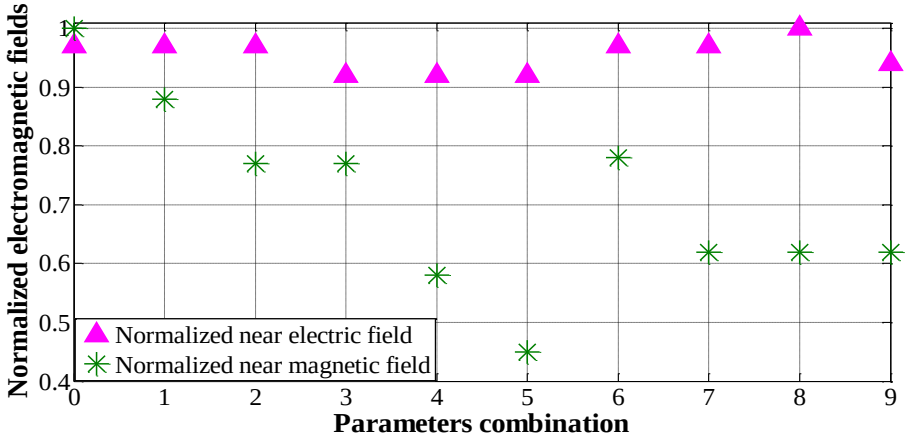

Fig. 10. The normalized near electric and magnetic fields for the parameter combinations summarized in Table 2.

The transmission coefficient decreases when the length (L_i) and height (h_i) of the inner ring are decreased as shown for the combinations number 1 and 2 because of a decrease in the near magnetic field. When the near magnetic field is decreased, the antenna gain (G_t) decreases. The percent of reduction in the transmission coefficient increases as the length and height of the inner ring decrease (see the results for combination number 2). Around double the decrease in the transmission coefficient is obtained in comparison with that for combination number 1 as each of *Li* and *hi* is further decreased by 1 mm for combination number 2 in comparison with that for combination number 1. Although the length and height of the inner ring for combinations number 2 and 3 are the same, 5% larger transmission coefficient is obtained for combination number 3. *G* is increased by 1 mm for this combination which causes the effective capacitance and near electric field to decrease. When the near electric field is decreased, larger power is transmitted outside the lossy medium to the receiving antenna which increases the power received by the external antenna and the

transmission coefficient correspondingly. A larger percentage of decrease in the transmission coefficient than that for other parameters can be obtained when the strip width is increased as can be seen for combinations number 4 to 7 in comparison with that for combinations number 1 to 3. The transmission coefficient decreases when the split width is decreased because the capacitance and near electric field are increased as shown for combination number 8. Smaller reduction in the transmission efficient is obtained for combination number 9 in comparison with that for combination number 8 because the split width is increased for this combination; and hence the near electric field is decreased accordingly.

Most of the reduction in the transmission coefficient is attributed to the reduction in the near magnetic field except for combination number 8. The reduction is caused by an increase in the near electric field in addition to the decrease in the near magnetic field. The reduction in the near electric field is small as 1 mm variation in the spacing between the rings (G) or the split width (S) is only examined.

The transmission coefficient for the fabricated antenna with optimum parameters is measured with and without the split rings layer at 403 MHz. The transmission coefficient is increased by 3 dB when the split rings layer is used. This assures the positive effect of the split ring layer.

5. CONCLUSIONS

In this paper, the effective parameters of a metallic layer based on rectangular split rings placed on a loop antenna inside a lossy medium are investigated. The effect of these parameters on the near electromagnetic fields, which play a major role in communication inside lossy media, is discussed and linked to the equivalent circuit parameters. The results in this paper indicate that optimizing these parameters can increase the power radiated out of the lossy medium. The transmission coefficient between a loop antenna in a lossy medium and an external loop antenna in a free space can be increased by up to 50% when the overall parameters of the inner split ring investigated in this paper are optimized. In the future, other structures and shapes of the split rings might be investigated.

REFERENCES

[1] M. Kod, J. Zhou, Y. Huang, M. Stanley, M. Hussein, A. Sohrab, R. Alrawashdeh, G. Wang, "Feasibility study of using the housing cases of implantable devices as antennas," *IEEE Access*, vol. 4, pp. 6939-6949, 2016.

[2] A. Massaccesi, P. Pirinoli, "Analysis of antennas for underwater applications," *Proceedings of The 2017 11th European Conference on Antennas and Propagation*, pp. 1907-1910, 2017.

[3] R. Moore, "Effects of a surrounding conducting medium on antenna analysis," *IEEE Transactions on Antennas and Propagation*, vol. 11, no. 3, pp. 216–225, 1963.

[4] F. Merli, *Implantable Antennas for Biomedical Applications*, Ph.D dissertation, EPFL University, Lausanne, Switzerland, 2011.

[5] R. Alrawashdeh, F. Alharazneh, S. Alsarayreh, and E. Aladaileh, "A novel flexible cloud shape loop antenna for muscle implantable devices," *Jordan Journal of Electrical Engineering*, vol. 5, no. 1, pp. 61-76, 2019.

[6] R. Alrawashdeh, "A review on wireless power transfer in free space and conducting lossy media," *Jordanian Journal of Computers and Information Technology*, vol. 3, no. 2, pp. 71-88, 2017.

[7] R. Alrawashdeh, *Implantable Antennas for Biomedical Applications*, Ph.D dissertation, University of Liverpool, Liverpool, U.K., 2015.

[8] Electromagnetic compatibility and Radio Spectrum Matters; Short Range Devices; Ultra Low Power Active Medical Implants and Peripheralsoperating in the frequency range 402 MHz to 405 MHz; Part 1 and Part 2, *European Telecommunications Standards Institute,* Std. EN 301 839-1/2 V1.3.1, 2007. < www.etsi.org>

[9] Electromagnetic compatibility and Radio Spectrum Matters; Short Range Devices; Ultra Low Power Active Medical Implants and Peripherals operating in the frequency range 401 MHz to 402 MHz and 405 MHz to 406 MHz; Part 1, *European Telecommunications Standards Institute,* Std. EN 302537-1V1.3.1, 2007. < www.etsi.org>

[10] D. Andreuccetti, R. Fossi, and C. Petrucci, "Calculation of the dielectric properties of body tissues in the frequency range 10 Hz - 100 GHz," *Institute for Applied Physics*, Italian National Research Council, Florence (Italy), 1997. Accessed: June 10, 2019. <http://niremf.ifac.cnr.it/tissprop/>

[11] R. Ziolkowski, A. Erentok, "Metamaterial-based efficient electrically small antennas," *IEEE Transactions on Antennas and Propagation*, vol. 54, no. 7, pp. 2113-2130, 2006.

[12] W. Hayt, J. Buck, *Engineering Electromagnetics*, USA, New York: McGraw Hill, 2012.

[13] *Understanding Inductance in the Real-World*, 2019. <https://interferencetechnology.com/understanding-inductance-real-world/>

[14] F. Gover, *Inductance Calculations*, USA, New York: Dover Publications, 1946.

[15] *CST-Computer Simulation Technolog,* 2013. <http://www.CST.com>

[16] *Agilent 85070E Dielectric Probe Kit*, 2013. <http://na.support.keysight.com/materials/help>

[17] R. Warty, M. Tofighi, U. Kawoos, A. Rosen, "Characterization of implantable antennas for intracranial pressure monitoring: Reflection by and transmission through a scalp phantom," *IEEE Transactions on Microwave Theory and Techniques*, vol. 56, no. 10, pp. 2366-2376, 2008.